$g_{9/2}$ neutron strength in the N=29 isotones and the $^{52}{ m Cr}(d,p)^{53}{ m Cr}$ reaction

L. A. Riley,¹ D. T. Simms,¹ L. T. Baby,² A. L. Conley,² P. D. Cottle,² J. Esparza,² K. Hanselman,² I. C. S. Hay,² M. Heinze,¹ B. Kelly,² K. W. Kemper,² G. W. McCann,² R. Renom,² M. Spieker,² and I. Wiedenhöver²

**Department of Physics and Astronomy,

*Ursinus College, Collegeville, PA 19426, USA**

²Department of Physics, Florida State University, Tallahassee, FL 32306, USA

(Dated: September 18, 2023)

Abstract

We performed a measurement of the 52 Cr $(d,p)^{53}$ Cr reaction at 16 MeV using the Florida State University Super-Enge Split-Pole Spectrograph (SE-SPS) and observed 26 states. While all of the states observed here had been seen in previous (d,p) experiments, we changed five L assignments from those reported previously and determined L values for nine states that had not had such assignments made previously.

The $g_{9/2}$ neutron strength observed in 53 Cr in the present work and in the N=29 isotones 49 Ca, 51 Ti, and 55 Fe via (d,p) reactions is much smaller than the sum rule for this strength. Most of the observed L=4 strength in these nuclei is located in states near 4 MeV excitation energy. The remaining $g_{9/2}$ strength may be located in the continuum or may be fragmented among many bound states. A covariant density functional theory calculation provides support for the hypothesis that the $g_{9/2}$ neutron orbit is unbound in 53 Cr. The $(\alpha, ^3$ He) reaction may provide a more sensitive probe for the missing $g_{9/2}$ neutron strength. In addition, particle- γ coincidence experiments may help resolve some remaining questions in this nucleus.

I. INTRODUCTION

As Maria Goeppert Mayer pointed out in 1949 [1], in nuclear shell structure the $1g_{9/2}$ orbit is the lowest-lying "intruder" orbit that is pushed down from its spin-orbit partner by the spin-orbit force into the next lower major shell, forming the fpg shell. The determination of the energy of the $1g_{9/2}$ neutron orbit is particularly important because of the role this orbit plays in the island of inversion phenomenon that occurs in isotopes near ⁶⁰Cr (see Ref. [2] and references therein). In this island of inversion, pairs of neutrons are promoted from fp orbits into the $g_{9/2}$ orbit, producing well-deformed shapes.

The nuclei in which it is most straightforward to determine the single neutron energies are the isotopes that have one neutron added to a closed shell (or one neutron subtracted from a closed shell). Nuclear reactions that deposit a single neutron onto a target with a closed neutron shell (or remove one neutron from a closed neutron shell) provide information on the energies of the single neutron orbits, even when the the single particle strength of these orbits is fragmented among several states in which the single neutron configurations mix with other nuclear excitations. By determining the single neutron strengths (or hole strengths) in these fragments, we can calculate the single neutron energy (or single neutron hole energy) as the centroid of the observed strength.

Here we present a new measurement of $1g_{9/2}$ neutron strength in the N=29 isotope ⁵³Cr via the ⁵²Cr(d, p)⁵³Cr reaction and compare this new experimental result with recent (d, p) results on the N=29 isotones ⁵¹Ti and ⁵⁵Fe. In these three nuclei, the sums of the $1g_{9/2}$ spectroscopic factors of the observed states are smaller than 0.5. It is possible that much of the $1g_{9/2}$ strength may be located above the single nucleon separation thresholds. This possibility is supported by a covariant functional theory calculation. Another possibility is that the $g_{9/2}$ strength is so fragmented that it is difficult to observe all of the fragments. The fragmentation of the $1g_{9/2}$ neutron strength in these isotones results at least in part from mixing with $J^{\pi} = 9/2^+$ states that occur because of the coupling of the octupole excitation in the core to the $2g_{3/2}$ ground states of the N=29 isotones.

II. EXPERIMENTAL DETAILS AND RESULTS

A deuteron beam, produced by a SNICS (Source of Negative Ions by Cesium Sputtering) source with a deuterated titanium cone, was accelerated to an energy of 16 MeV by the 9 MV Super FN Tandem Van de Graaff Accelerator at the John D. Fox Superconducting Accelerator Laboratory at Florida State University. The beam was delivered to a natural Cr target of thickness 300 μ g/cm² on a 20 μ g/cm² carbon backing that was mounted in the target chamber of the Super-Enge Split-Pole Spectrograph. The natural abundance of 52 Cr is 84%. The spectrograph, which accepted a solid angle of 4.6 msr, was rotated from scattering angles of 15° to 50° at increments of 5° to measure angular distributions of protons from the 52 Cr(d, p) 53 Cr reaction. Further details of the experimental setup are described in Ref. [3].

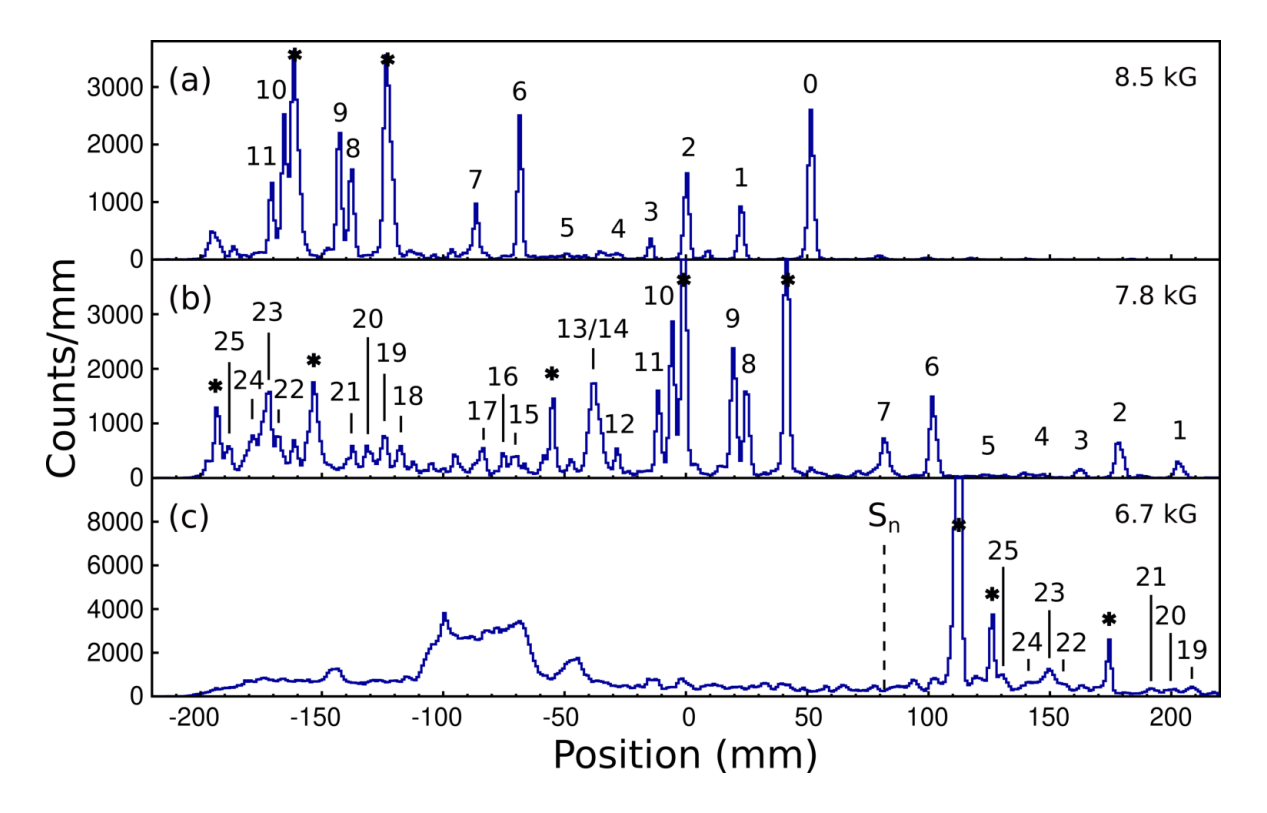


FIG. 1. (Color online) Proton momentum spectra at a laboratory angle of 25° for the three magnetic field settings used in the spectrograph for this experiment. Peaks from ⁵³Cr are labeled with the numbers listed in Table I. Contaminant peaks are labeled with asterisks. The spectra are shown as a function of position in the focal plane detector.

Proton momentum spectra collected at a scattering angle of 25° and with the three

spectrograph magnetic field settings used in this experiment are shown in Figure 1.

TABLE I: Excitation energies from the present work and Ref. [4], angular-momentum transfer, and J^{π} assignments, single-neutron orbits used for the FRESCO [5] analysis, and the spectroscopic factors for states of 53 Cr populated in the present work. Established J^{π} assignments are from Ref. [4]. Tentative J^{π} assignments based on L values determined in the present work are discussed in the text. When more than one possible orbit is given for a state, the spectroscopic factors assuming both orbits are shown.

Label	$E_x \text{ (keV)}$	$E_x ext{ (keV)}$	L	J^{π}	orbit	S	Comments
]	Present Work	Ref. [4]					
0	0(3)	0	1	$\frac{3}{2}$	$2p_{3/2}$	0.33(2)	
1	564(2)	564.03(4)	1	$\frac{1}{2}^{-}$	$2p_{1/2}$	0.21(2)	
2	1006(2)		3	$\frac{5}{2}$	$1f_{5/2}$	0.21(1)	
3	1289(2)	1289.52(7)	3	$\frac{7}{2}^{-}$	$1f_{7/2}$	0.032(3)	
4	1549(11)	1536.62(7)	3	$\frac{7}{2}^{-}$	$1f_{7/2}$	0.008(1)	
5	1949(12)						Ref. [4] reports no L assignment.
						0.055(12)	
6	2317(4)	2320.71(21)	1	$\frac{3}{2}^{-}$	$2p_{3/2}$	0.15(1)	
7	2664(6)	2656.5(3)	3	$\frac{5}{2}$	$1f_{5/2}$	0.11(1)	
8	3619(9)	3616.51(18)	1	$\frac{1}{2}^{-}$	$2p_{1/2}$	0.20(2)	
9	3712(10)	3706.5(15)					
10	4170(11)	4135.1(6)	2	$\frac{5}{2}$ +	$2d_{5/2}$	0.054(4)	Ref. [4] reports $J^{\pi} = 5/2^+, 3/2^+$
11	4268(10)	4230.5(7)	2	$\frac{5}{2}$ +	$2d_{5/2}$	0.027(2)	Ref. [4] reports $J^{\pi} = 5/2^+, 3/2^+$
12	4562(10)	4551(10)	2	$\frac{5}{2}$ +	$2d_{5/2}$	0.011(1)	Ref. [4] reports no L assignment.
13	4683(10)	4690(7)	1	$\frac{1}{2}^{-}$	$2p_{1/2}$	0.10(2)	Ref. [4] reports $J^{\pi} = 1/2^+$
				$\frac{3}{2}$	$2p_{3/2}$	0.050(10)	
14	4740(10)	4745(7)	3	$\frac{5}{2}^{-}$	$1f_{5/2}$	0.15(2)	Ref. [4] reports no L assignment.
15	5306(10)	5310(10)	3	$\frac{5}{2}$	$1f_{5/2}$	0.026(4)	Ref. $[4]$ reports no L assignment.
16	5379(10)	5397(10)	3	$\frac{1}{2}$	$1f_{5/2}$	0.020(4)	Ref. [4] reports $J^{\pi} = 1/2^{-}, 3/2^{-}$.
17	5529(10)	5557(10)	1	$\frac{1}{2}$	$2p_{1/2}$	0.043(6)	
			1	$\frac{1}{2}$	$2p_{3/2}$	0.022(3)	
18	6123(10)	6114(10)		_	,		Ref. $[4]$ reports no L assignment.
19	6230(10)	6231(10)					Ref. [4] reports $J^{\pi} = (1/2^{+})$.
20	6342(10)	6335(10)		_			Ref. $[4]$ reports no L assignment.
		Co	onti	inu	$\stackrel{\cdot}{\text{ed on}}$	next page	

TABLE I — continued from previous page

Label	$E_x ext{ (keV)}$	$E_x ext{ (keV)}$	$L J^{\pi}$	orbit	S	Comments
	Present Work	Ref. [4]				
21	6460(10)	6460(10)	$1 \frac{1}{2}^{-}$	$2p_{1/2}$	0.044(3)	Ref. [4] reports no L assignment
			$1\frac{3}{2}^{-}$	$2p_{3/2}$	0.022(2)	
22	6961(10)	6961(10)	$1 \frac{1}{2}^{-}$	$2p_{1/2}$	0.032(8)	Ref. [4] reports $J^{\pi} = 1/2^{+}$.
			$1 \frac{3}{2}^{-}$	$2p_{3/2}$	0.016(4)	
23	7045(12)	7056(10)	$3\frac{5}{2}^{-}$	$1f_{5/2}$	0.058(4)	Ref. [4] reports no L assignment
24	7165(10)	7167(10)	$3\frac{5}{2}^{-}$	$1f_{5/2}$	0.022(3)	Ref. [4] reports $J^{\pi} = 1/2^{+}$.
25	7329(10)	7321(10)	$2 \frac{5}{2}^{+}$	$2d_{5/2}$	0.018(1)	Ref. [4] reports no L assignment

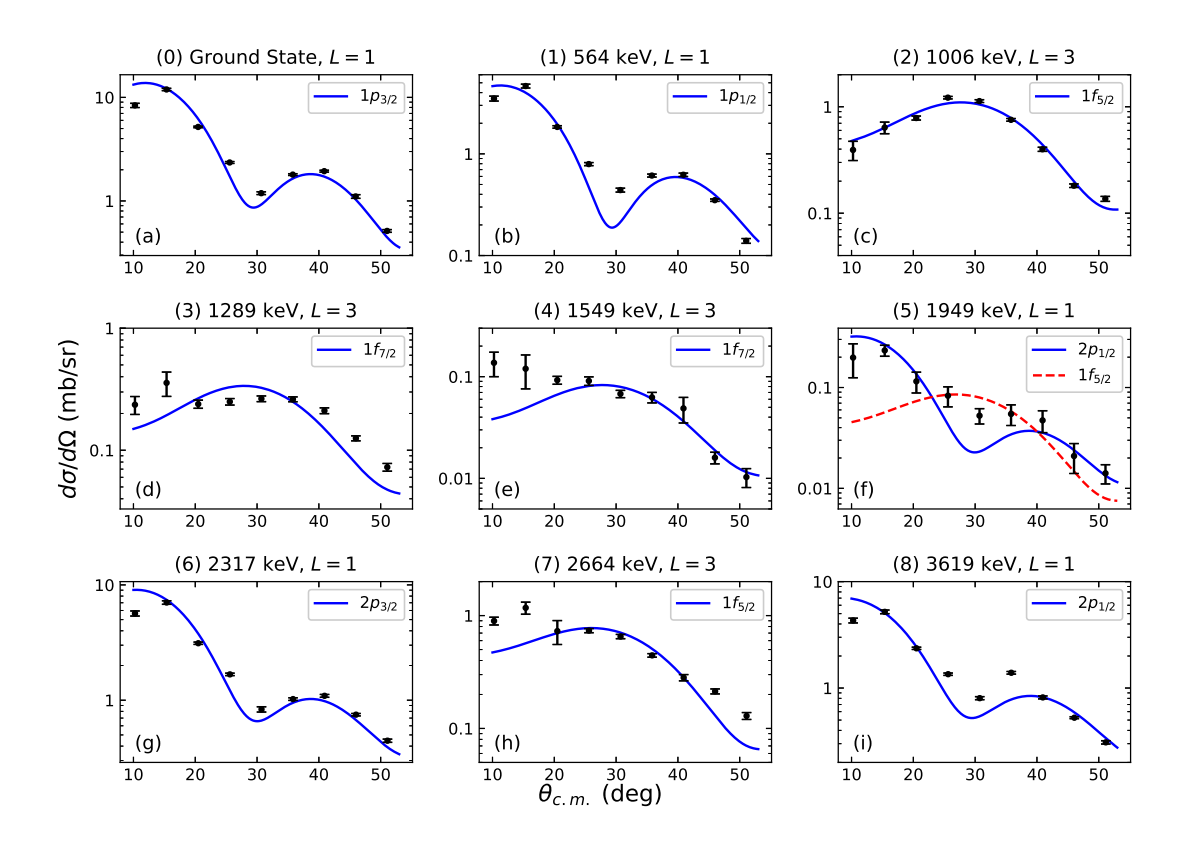


FIG. 2. (Color online) Measured proton angular distributions from the 52 Cr $(d,p)^{53}$ Cr reaction compared with FRESCO [5] calculations described in the text. Panels (a) to (i) correspond to the states 0-8 in Table I.

The magnetic rigidity spectrum measured at each scattering angle was fit using a linear combination of Gaussian functions with a cubic background. The proton yields corresponding to each state in ⁵³Cr were used to produce the measured proton angular distributions

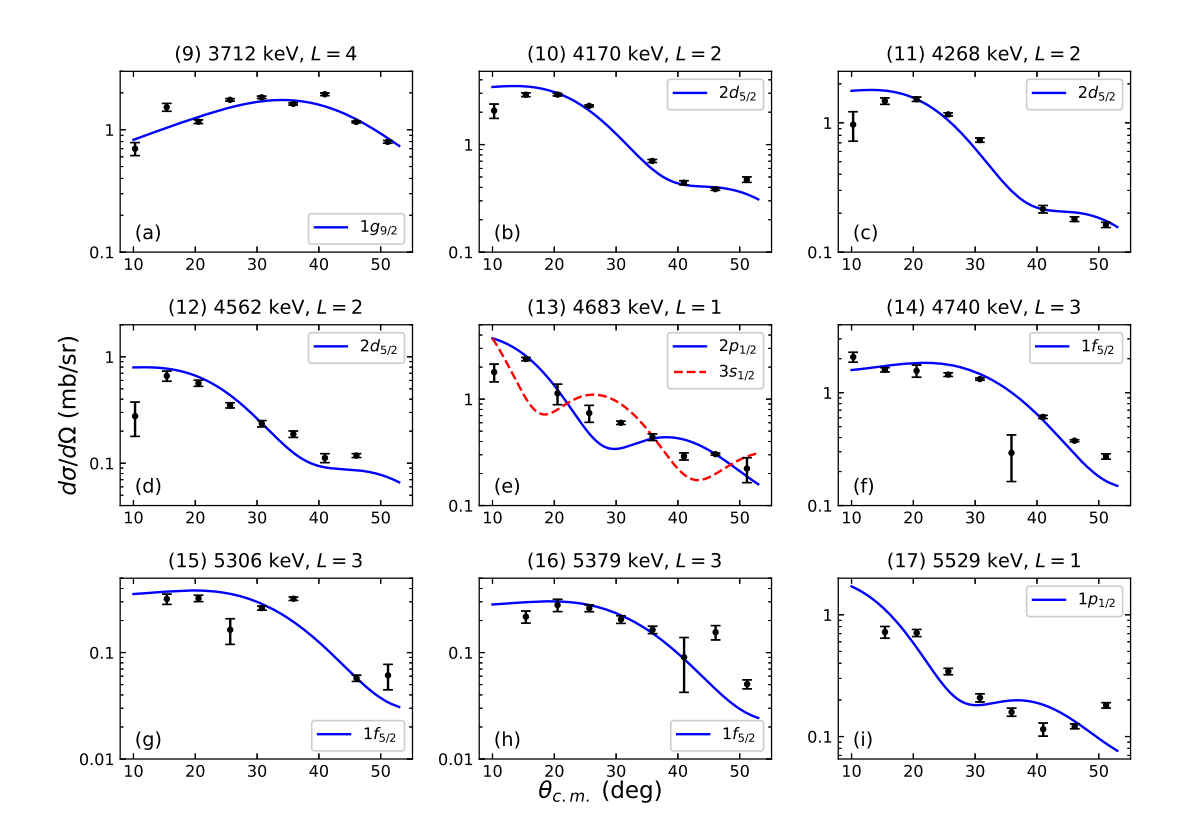


FIG. 3. (Color online) Measured proton angular distributions from the 52 Cr $(d,p)^{53}$ Cr reaction compared with FRESCO [5] calculations described in the text. Panels (a) to (i) correspond to the states 9-17 in Table I.

TABLE II. Optical potential parameters used in FRESCO [5] calculations in the present work determined using Refs. [6] and [7] as described in the text.

	V_V	r_V	a_V	W_V	r_W	a_W	W_D	r_D	a_D	V_{so}	W_{so}	r_{so}	a_{so}	r_C
	(MeV)	(fm)	(fm)	(MeV)	(fm)	(fm)	(MeV)	(fm)	(fm)	(MeV)	(MeV)	(fm)	(fm)	(fm)
$d+^{52}Cr$	104.3	1.195	0.702	1.23	1.197	0.702	14.98	1.283	0.583	11.31	-0.13	1.013	0.621	1.25
$\mathrm{p}+^{53}\mathrm{Cr}$	46.4	1.196	0.670	1.30	1.197	0.670	6.88	1.283	0.553	5.48	-0.08	1.013	0.590	1.25

shown in Figs. 2-4. The absolute cross sections were determined to be accurate to an uncertainty of 15%, with contributions from uncertainties in charge integration, target thickness and solid angle.

The B ρ calibration (which gives the energy calibration) is based on adopted energies from Ref. [4]. The uncertainties are statistical—from both the peak positions from the fit and the propagated uncertainties in the calibration parameters, except in cases in which this results in a smaller uncertainty than that given in Ref. [4]. In those cases, we report the

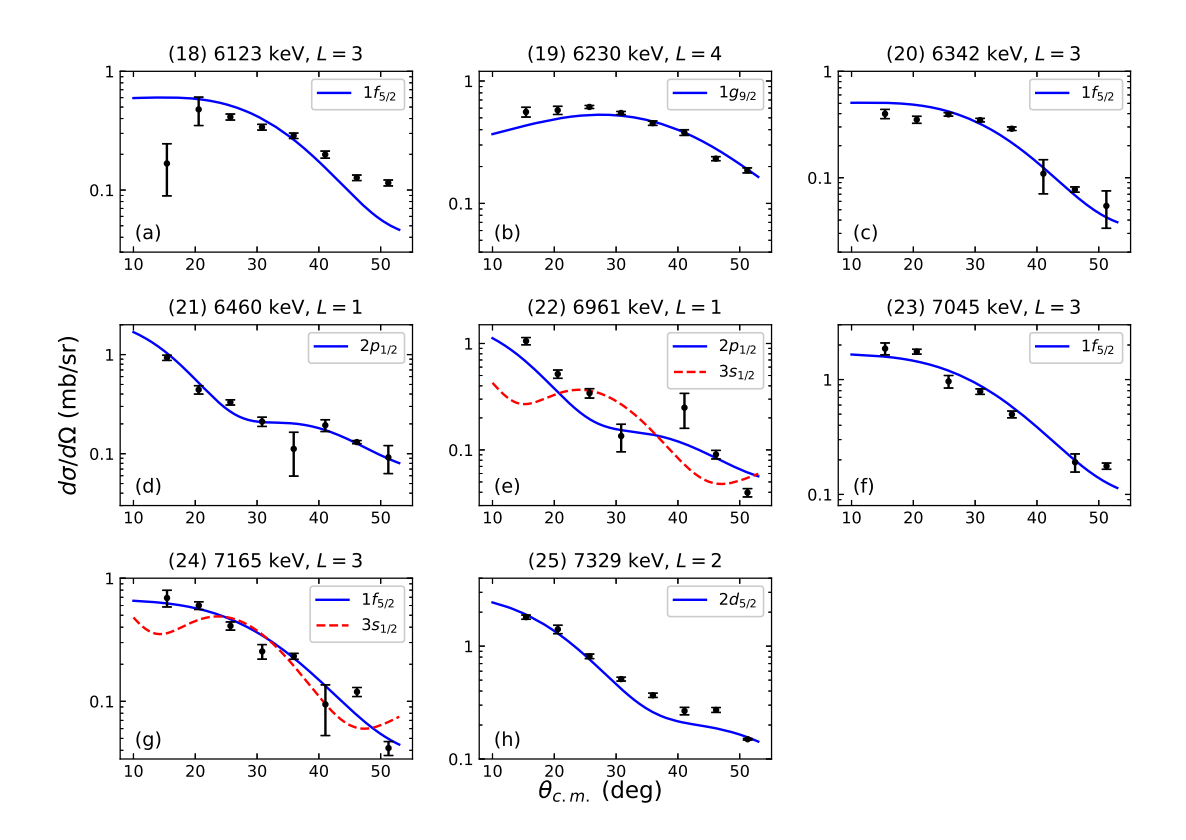


FIG. 4. (Color online) Measured proton angular distributions from the 52 Cr $(d,p)^{53}$ Cr reaction compared with FRESCO [5] calculations described in the text. Panels (a) to (h) correspond to the states 18-25 in Table I.

uncertainty from Ref. [4].

To extract spectroscopic factors from the present angular distributions, calculations that use the adiabatic approach for generating the entrance channel deuteron optical potentials (as developed by Johnson and Soper [6]) were used. The potential was produced using the formulation of Wales and Johnson [7]. Its use takes into account the possibility of deuteron breakup and has been shown to provide a more consistent analysis as a function of bombarding energy [8] as well as across a large number of (d, p) and (p, d) transfer reactions on Z = 3 - 24 target nuclei [9]. The proton-neutron and neutron-nucleus global optical potential parameters of Koning and Delaroche [10] were used to produce the deuteron potential as well as the proton-nucleus optical potential parameters needed for the exit channel of the (d, p) transfer calculations, in keeping with the nomenclature of Ref. [8]. The angular momentum transfer and spectroscopic factors found in Table I were determined by scaling these calculations, made with the FRESCO code [5], to the proton angular distributions.

Optical potential parameters are listed in Table II. The overlaps between 53 Cr and 52 Cr+n were calculated using binding potentials of Woods-Saxon form whose depth was varied to reproduce the given state's binding energy with geometry parameters of $r_0 = 1.25$ fm and $a_0 = 0.65$ fm and a Thomas spin-orbit term of strength $V_{so} = 6$ MeV that was not varied.

We observed 26 states in 53 Cr, all of which had been previously observed in 52 Cr(d,p) measurements [4]. However in five of these states, the transferred angular momentum L determined here is different from that given in Ref. [4]. For the 4683 keV state, Ref. [4] reported $J^{\pi}=1/2^{+}$, corresponding to L=0. We determined that the 4683 keV state is populated via L=1 transfer instead by comparing the chi-square value of 24.2 for the best L=1 fit to the chi-square value of 83.1 to the best L=0 fit. Similarly, we changed: the L assignment for the 5379 keV state to L=3 (chi-square of 7.0) from the L=1 value given in Ref. [4] (chi-square of 34.7); the assignment for the 6230 keV state to L=4 (chi-square of 8.4) from the L=0 value given in Ref. [4] (chi-square of 13.2) from the L=0 value given in Ref. [4] (chi-square of 23.6); and, the assignment for the 7165 keV state to L=3 (chi-square of 4.0) from the L=0 value given in Ref. [4] (chi-square of 12.3).

In another nine states, we made L assignments for the first time. Of these nine states, the most difficult to assign was the 1949 keV state. As shown in Fig. 2, we performed best fits for L=1 and L=3 to the data. A comparison of the chi-square values for L=1 (2.6) and L=3 (6.5) favored the L=1 assignment.

Distinguishing between spin-orbit partners like $p_{3/2}$ - $p_{1/2}$ and $f_{7/2}$ - $f_{5/2}$ with the (d, p) reaction generally requires the measurement of analyzing powers with a polarized deuteron beam, which was not available for the present experiment. Therefore, unless there is other experimental evidence available for L=1 states to distinguish between $J^{\pi}=3/2^-$ and $1/2^-$ assignments, we list both possibilities (and spectroscopic factors for both possibilities) in Table I. We approached L=3 states differently because the $f_{7/2}$ orbit lies below the N=28 shell closure. Aside from the 1289 and 1549 keV states, we assumed that states for which angular distributions were best fit with L=3 were $J^{\pi}=5/2^-$ states (corresponding to the $f_{5/2}$ neutron orbit).

Only two of the states observed here have L=4, corresponding to neutron transfer into the $g_{9/2}$ neutron orbit. The distribution of $g_{9/2}$ strength in the N=29 isotones ⁴⁹Ca, ⁵¹Ti, ⁵³Cr, and ⁵⁵Fe is compared to that of the $f_{5/2}$ strength in Figure 5 and discussed in the next

section.

III. DISCUSSION

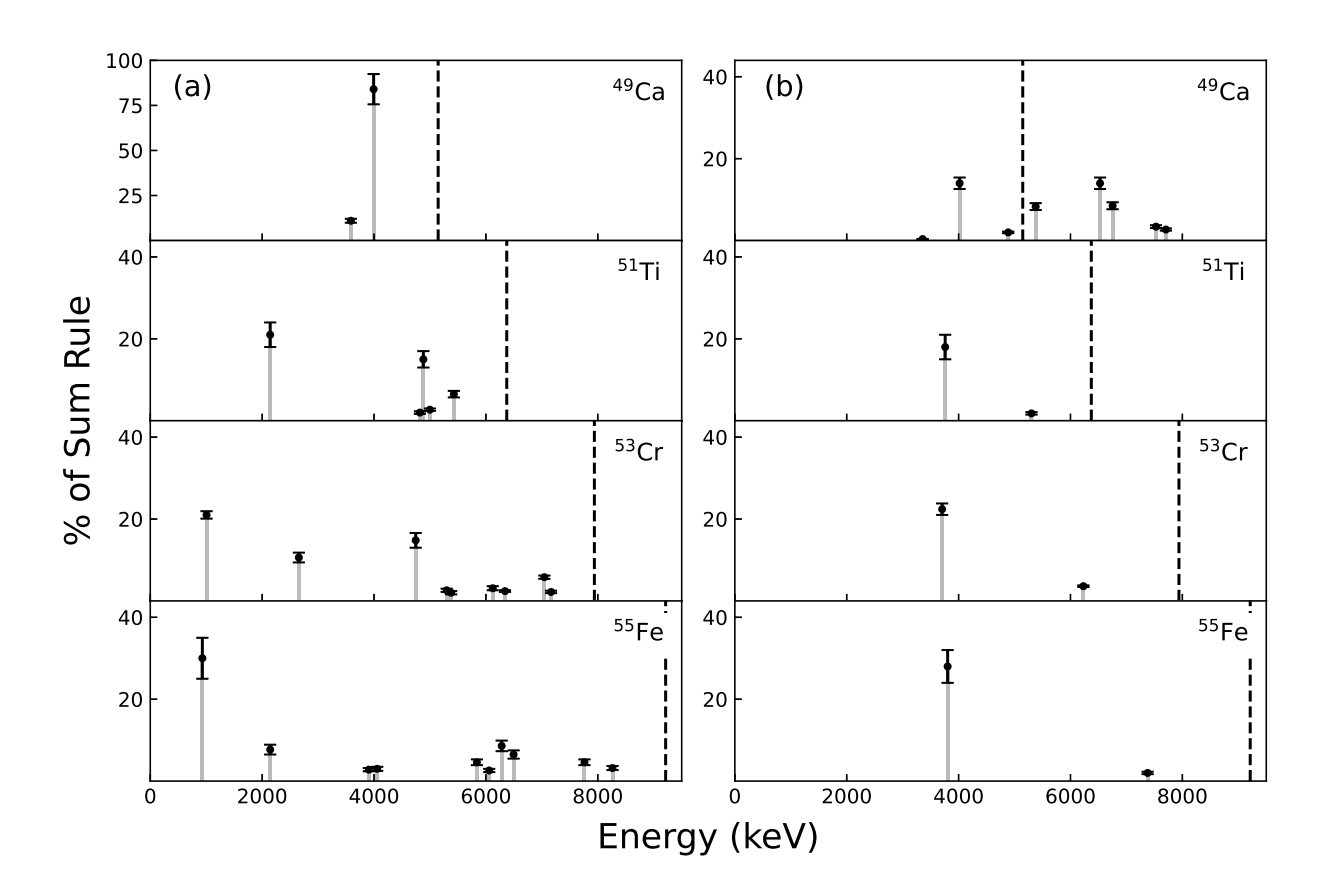


FIG. 5. The $f_{5/2}$ (panel a) and $g_{9/2}$ (panel b) strength distributions observed in the N=29 even-Z isotones from Ca to Fe. A spectroscopic factor of 1 would correspond to 100% of the sum rule strength. The dashed lines show the particle decay thresholds, which are the single neutron separation energies in 49 Ca, 51 Ti and 53 Cr and the single proton separation energy in 55 Fe. The data for 53 Cr are from the present work. Data for 49 Ca are from [11]; for 51 Ti from [3]; and for 55 Fe from [12]. Single nucleon separation energies are from Refs. [4, 13–15].

In (d,p) studies of the even-Z N=29 isotones ⁴⁹Ca [11], ⁵¹Ti [3] and ⁵⁵Fe [12], the total spectroscopic strengths observed for the $g_{9/2}$ neutron orbit are much smaller than the strengths observed for the $f_{5/2}$ neutron orbit. While distinguishing between $p_{3/2}$ and $p_{1/2}$

states can be difficult without analyzing power data from reactions with polarized deuteron beams, nearly all of the L=3 strength observed in (d,p) reactions in these nuclei can be attributed to the $f_{5/2}$ orbit. Therefore, comparing the observed $g_{9/2}$ strength with that of the $f_{5/2}$ neutron orbit is the best way of determining whether the $g_{9/2}$ strength is anomalously small.

In the ${}^{48}\text{Ca}(d,p){}^{49}\text{Ca}$ study at 56 MeV by Uozumi et al. [11], the sum of the spectroscopic factors for the observed $f_{5/2}$ states is 0.97, while the sum of the $g_{9/2}$ spectroscopic strengths is 0.53. Incidentally, Uozumi et al. used a polarized deuteron beam so they were able to distinguish between $p_{3/2}$ and $p_{1/2}$ neutron states. The sum of the spectroscopic factors for the $p_{3/2}$ states Uozumi et al. observed was 0.97, while the sum of the spectroscopic factors they obtained for $p_{1/2}$ was 1.03.

The most recent (d, p) study of ⁵¹Ti was performed by Riley *et al.* at 16 MeV [3]. In this study, the sum of the spectroscopic factors for the $f_{5/2}$ states was 0.47(4), while the corresponding sum for the $g_{9/2}$ states was 0.20(3).

In ⁵⁵Fe, Riley *et al.* [12] used the (d, p) reaction at 16 MeV to identify several $f_{5/2}$ states that gave a summed spectroscopic factor of 0.74(6). In the same study, the sum of spectroscopic factors for $g_{9/2}$ was 0.32(4).

In all three of the cases, the observed $g_{9/2}$ strength was less than 60% of the $f_{5/2}$ strength.

In the present study of 53 Cr, the sum of the spectroscopic factors listed for the two states listed in Table 1 that are populated via L=4 transfer (and which are therefore presumed to be $g_{9/2}$ neutron states) is 0.26(1). However, the sum of the spectroscopic factors for the $f_{5/2}$ states measured in the present experiment is 0.57(3). In 53 Cr, as in 49 Ca, 51 Ti and 55 Fe, the observed $g_{9/2}$ strength is much smaller than the observed $f_{5/2}$ strength.

The distributions of $f_{5/2}$ and $g_{9/2}$ strength in these four nuclei are summarized in Figure 5.

It is clear that in all four of these N=29 isotones, the $g_{9/2}$ neutron strength is fragmenting by mixing with other $J^{\pi}=9/2^+$ states and that this is resulting in a significant share of the $g_{9/2}$ strength being concentrated in a state near 4.0 MeV. One way to produce a $9/2^+$ state in these N=29 isotones is to couple the $p_{3/2}$ neutron, which is the lowest valence neutron orbit in these isotones and which sets the $3/2^-$ ground state J^{π} values in all four of them, to the low energy octupole state in the N=28 core nucleus. In ⁴⁹Ca, Montanari et al. [16] demonstrated that the $9/2^+$ state at 4017.5 keV has a large octupole component.

They populated ⁴⁹Ca via a single-neutron transfer reactions with a ⁴⁸Ca beam impinging on ⁶⁴Ni and ²⁰⁸Pb targets and used a large array of high-resolution γ -ray detectors to measure lifetimes with the differential recoil distance Doppler shift method. They were able to determine that the reduced matrix element B(E3) for the decay of the 4017.5 keV 9/2⁺ state to the 3/2⁻ ground state is 8(2) W.u. This result overlaps with the value of 8.4 W.u. (+4.3, -3.5) given in [17] for the transition from the lowest 3₁⁻ state in the core nucleus ⁴⁸Ca (which is located at 4507 keV) to the ground state. But in addition, Uozumi *et al.* [11] determined that the 4017.5 keV state in ⁴⁹Ca has a $g_{9/2}$ neutron spectroscopic factor of 0.14. So clearly this state has a significant $g_{9/2}$ single neutron component as well.

The situations in 51 Ti, 53 Cr and 55 Fe appear to be similar to that in 49 Ca. In 51 Ti, there is a $9/2^+$ state at 3771 keV that has a $g_{9/2}$ spectroscopic factor of 0.18(3) [3]. In the 50 Ti core nucleus, the 3^- state that appears to be the strongest low energy octupole state occurs at 4410 keV [18]. The lowest $9/2^+$ state in 53 Cr, which occurs at 3706 keV and has a $g_{9/2}$ spectroscopic factor of 0.22(3), can be compared in energy to the 3_1^- state in 52 Cr, which occurs at 4470 keV [19]. In 55 Fe, the lowest $9/2^+$ state is found at 3804 keV and has a $g_{9/2}$ spectroscopic factor of 0.28(4) [12]. The 3_1^- state in the core nucleus 54 Fe occurs at 4782 keV [20].

Mixing between a $g_{9/2}$ single neutron state and a $p_{3/2} \otimes 3_1^-$ state that occurs at a lower energy than the unperturbed $g_{9/2}$ neutron state would certainly result in what we see experimentally in ⁴⁹Ca and what we likely have in ⁵¹Ti, ⁵³Cr and ⁵⁵Fe as well - a $9/2^+$ state that has a somewhat collective B(E3) value for decay to the ground state and a $g_{9/2}$ spectroscopic factor that is significant but much smaller than 1.0. But this two-state mixing scenario would also result in another state at higher energy than the unperturbed $g_{9/2}$ single neutron state that carries most of the $g_{9/2}$ strength. At present, there is no evidence for such a state or even a high-lying concentration of L=4 strength in the four N=29 isotones being discussed here.

The present 53 Cr experiment and the recent experiments on 51 Ti [3] and 55 Fe [12] only searched for states up to the particle thresholds (6372 keV in 51 Ti, 7939 keV in 53 Cr and 9213 keV in 55 Fe [4, 14, 15]). Therefore, it is at least possible that the bulk of the $g_{9/2}$ strength is in the continuum.

The possibility that the bulk of the $g_{9/2}$ neutron strength is in the continuum is given credibility by the results of a calculation performed in the framework of covariant density

functional theory. This calculation of the binding energies of the $p_{3/2}$, $p_{1/2}$, $f_{5/2}$ and $g_{9/2}$ neutron orbits in ⁴⁸Ca, ⁵⁰Ti, ⁵²Cr and ⁵⁴Fe uses the covariant energy density functional FSUGarnet [21] and is described in detail in Ref. [3].

Table III shows that the calculations for the $p_{3/2}$, $p_{1/2}$ and $f_{5/2}$ binding energies in 48 Ca, 50 Ti and 54 Fe are within 0.7 MeV of the experimental binding energies for these orbits in 49 Ca, 51 Ti and 55 Ti. That is, the calculation provides a reasonable description of the binding energies of these neutron orbits. The same calculation predicts that the $g_{9/2}$ neutron orbit is unbound in 48 Ca, 50 Ti and 52 Cr, and bound by only 1.4 MeV in 54 Fe.

It is also possible that the $g_{9/2}$ neutron orbit is bound and that the strength is located in bound states, but the strength is so fragmented that the present experiments do not have the sensitivity necessary to observe it.

In either case, finding the "missing" $g_{9/2}$ neutron strength would require a more sensitive experimental probe than the (d, p) reaction with 16 MeV deuterons used in the present work and in Refs. [3, 12]. As noted by (for example) Szwec et al. [22], single nucleon transfer reactions vary in their sensitivities to populating orbits of different L values. In the reaction studied in the present work, the difference in the angular momenta of the incoming deuteron and outgoing proton is $1.0\hbar$. Therefore, this reaction is most sensitive to the $p_{3/2}$ and $p_{1/2}$ orbits. In contrast, the $(\alpha,^3\text{He})$ reaction is more sensitive to orbits with higher angular momenta. For example, the difference between the angular momenta of the incoming α -particle and outgoing ^3He nucleus in the $^{52}\text{Cr}(\alpha,^3\text{He})^{53}\text{Cr}$ reaction at 32 MeV (an energy that is accessible at the Fox Laboratory) is $6.6\hbar$. Consequently, this reaction would be more sensitive to neutron orbits having larger orbital angular momenta such as $g_{9/2}$.

Detecting γ -rays in coincidence with particle detection in the SE-SPS could provide additional selectivity that would be especially helpful in reactions like the one studied here in which the spectrum of excited states is crowded. CeBr₃ scintillators can provide resolution of 4% or better at energies above 500 keV while providing resilience in the presence of large neutron fluxes like those present during (d, p) experiments [23]. Five CeBr₃ detectors are already available for particle- γ coincidence experiments at the SE-SPS.

TABLE III. Experimental binding energies in the even-Z N=29 isotones and theoretical binding energies for the neighboring N=28 isotones calculated using the covariant functional theory described in the text. All energies in MeV. Data taken from [3, 4, 11-15] and the present work.

	$p_{3/2}$ expt	$p_{1/2}$ expt	$f_{5/2}$ expt	$p_{3/2}$ theory	,	,	$g_{9/2}$ theory
49Ca	4.60(7)	2.87(3)	1.19(1)	4.37	3.06	1.31	unbound
$^{51}\mathrm{Ti}$	5.80(15)	4.34(22)	2.63(10)	5.51	4.21		unbound
	6.05(114) 8.22(11)	` '	` /		5.39 6.58	4.73 6.44	unbound 1.42

IV. CONCLUSIONS

We performed a measurement of the 52 Cr $(d,p)^{53}$ Cr reaction at 16 MeV using the FSU SE-SPS. All 26 states we observed had been seen in previous (d,p) measurements. However, we changed five L assignments from those reported previously. In addition, we determined L values for nine states that were previously observed but for which no L assignment had been made.

The $g_{9/2}$ neutron strength observed via the (d, p) reaction is much less than expected in the N=29 isotones 49 Ca, 51 Ti, 53 Cr and 55 Fe. Most of the observed $g_{9/2}$ strength in these nuclei is located in states near 4 MeV. The remaining $g_{9/2}$ strength may be located in the continuum. This possibility is supported by the convariant functional theory calculation presented here. Alternatively, the $g_{9/2}$ strength may be fragmented among many bound states. The $(\alpha,^3$ He) reaction may provide a more sensitive probe for the missing $g_{9/2}$ neutron strength. In addition, particle- γ coincidence experiments with CeBr₃ detectors may provide additional sensitivity for identifying these missing fragments.

ACKNOWLEDGMENTS

This work was supported by the National Science Foundation through grant number PHY-2012522. We thank Jorge Piekarewicz for the covariant density functional theory

calculations.

- [1] M. G. Mayer, Phys. Rev. **75**, 1969 (1949).
- [2] A. Gade, R. V. F. Janssens, D. Bazin, P. Farris, A. M. Hill, S. M. Lenzi, J. Li, D. Little, B. Longfellow, F. Nowacki, A. Poves, D. Rhodes, J. A. Tostevin, and D. Weisshaar, Phys. Rev. C 103, 014314 (2021).
- [3] L. A. Riley, J. M. Nebel-Crosson, K. T. Macon, G. W. McCann, L. T. Baby, D. Caussyn, P. D. Cottle, J. Esparza, K. Hanselman, K. W. Kemper, E. Temanson, and I. Wiedenhöver, Phys. Rev. C 103, 064309 (2021).
- [4] H. Junde, Nuclear Data Sheets 110, 2689 (2009).
- [5] I. J. Thompson, Computer Physics Reports 7, 167 (1988).
- [6] R. C. Johnson and P. J. R. Soper, Phys. Rev. C 1, 976 (1970).
- [7] G. Wales and R. Johnson, Nuclear Physics A **274**, 168 (1976).
- [8] F. Delaunay, F. M. Nunes, W. G. Lynch, and M. B. Tsang, Phys. Rev. C 72, 014610 (2005).
- [9] J. Lee, M. B. Tsang, and W. G. Lynch, Phys. Rev. C 75, 064320 (2007).
- [10] A. J. Koning and J. P. Delaroche, Nuclear Physics A **713**, 231 (2003).
- [11] Y. Uozumi, O. Iwamoto, S. Widodo, A. Nohtomi, T. Sakae, M. Matoba, M. Nakano, T. Maki, and N. Koori, Nuclear Physics A 576, 123 (1994).
- [12] L. A. Riley, I. C. S. Hay, L. T. Baby, A. L. Conley, P. D. Cottle, J. Esparza, K. Hanselman, B. Kelly, K. W. Kemper, K. T. Macon, G. W. McCann, M. W. Quirin, R. Renom, R. L. Saunders, M. Spieker, and I. Wiedenhöver, Phys. Rev. C 106, 064308 (2022).
- [13] T. Burrows, Nuclear Data Sheets **109**, 1879 (2008).
- [14] J. Wang and X. Huang, Nuclear Data Sheets **144**, 1 (2017).
- [15] H. Junde, Nuclear Data Sheets **109**, 787 (2008).
- [16] D. Montanari, S. Leoni, D. Mengoni, J. J. Valiente-Dobon, G. Benzoni, N. Blasi, G. Bocchi, P. F. Bortignon, S. Bottoni, A. Bracco, F. Camera, P. Casati, G. Colò, A. Corsi, F. C. L. Crespi, B. Million, R. Nicolini, O. Wieland, D. Bazzacco, E. Farnea, G. Germogli, A. Gottardo, S. M. Lenzi, S. Lunardi, R. Menegazzo, G. Montagnoli, F. Recchia, F. Scarlassara, C. Ur, L. Corradi, G. de Angelis, E. Fioretto, D. R. Napoli, R. Orlandi, E. Sahin, A. M. Stefanini, R. P. Singh, A. Gadea, S. Szilner, M. Kmiecik, A. Maj, W. Meczynski, A. Dewald, T. Pissulla,

- and G. Pollarolo, Phys. Rev. C 85, 044301 (2012).
- [17] J. Chen, Nuclear Data Sheets **179**, 1 (2022).
- [18] J. Chen and B. Singh, Nuclear Data Sheets **157**, 1 (2019).
- [19] Y. Dong and H. Junde, Nuclear Data Sheets 128, 185 (2015).
- [20] Y. Dong and H. Junde, Nuclear Data Sheets 121, 1 (2014).
- [21] W.-C. Chen and J. Piekarewicz, Physics Letters B **748**, 284 (2015).
- [22] S. V. Szwec, D. K. Sharp, B. P. Kay, S. J. Freeman, J. P. Schiffer, P. Adsley, C. Binnersley, N. de Séréville, T. Faestermann, R. F. Garcia Ruiz, F. Hammache, R. Hertenberger, A. Meyer, C. Portail, I. Stefan, A. Vernon, S. Wilkins, and H.-F. Wirth, Phys. Rev. C 104, 054308 (2021).
- [23] M. Spieker, private communication (2023).